PCCP

Accepted Manuscript

ROYAL SOCIETY OF CHEMISTRY

www.rsc.org/pccp

PCCP

ARTICLE

Multicomponent Kinetic Analysis and Theoretical Studies on the Phenolic Intermediates in the Oxidation of Eugenol and Isoeugenol Catalyzed by Laccase

Received 00th January 20xx,
Accepted 00th January 20xx

DOI: 10.1039/x0xx00000x

www.rsc.org/

Yan-Bing Qi,‡[a] Xiao-Lei Wang,‡[a] Ting Shi,[a] Shuchang Liu,[a] Zhen-Hao Xu,[a] Xiqing Li,[b] Xuling Shi,[c] Ping Xu,[a] Yi-Lei Zhao*[a]

Laccase catalyzes oxidation of natural phenols and thereby is believed to initialize reactions in lignification and delignification. Numerous phenolic mediators have also been applied in laccase-mediator systems. However, reaction details after the primary O-H rupture of phenols remain obscure. In this work two types of isomeric phenols, **EUG** (eugenol) and **ISO** (*trans-/cis*-isoeugenol), were used as chemical probes to explore the enzymatic reaction pathways, with the combined methods of time-resolved UV-Vis absorption spectra, MCR-ALS, HPLC-MS, and quantum mechanical (QM) calculations. It has been found that the **EUG**-consuming rate is linear to its concentration, while the **ISO** not. Besides, an *o*-methoxy quinone methide intermediate, (E/Z)-4-allylidene-2-methoxycyclohexa-2,5-dienone, was evidenced in the case of **EUG** with the UV-Vis measurement, mass spectra and TD-DFT calculations; in contrast, an **ISO**-generating phenoxyl radical, (E/Z)-2-methoxy-4-(prop-1-en-1-yl) phenoxyl radical, was identified in the case of **ISO**. Furthermore, QM calculations indicated that the **EUG**-generating phenoxyl radical (*O*-centered radical) can easily transform to allylic radical (*C*-centered radical) by hydrogen atom transfer (HAT) with a calculated activation enthalpy of 5.3 kcal/mol and then be fast oxidized to the observed eugenol quinone methide, rather than a *O*-radical alkene addition with barriers above 12.8 kcal/mol. Contrastively, the **ISO**-generating phenoxyl radical directly undergoes a radical coupling (RC) process, with a barrier of 4.8 kcal/mol, while the HAT isomerization between *O*- and *C*-centered radicals has a higher reaction barrier of 8.0 kcal/mol. The electronic conjugation of benzyl-type radical and aromatic allylic radical leads to differentiation of the two pathways. These results imply that competitive reaction pathways exist for the nascent reactive intermediates generated in the laccase-catalyzed oxidation of natural phenols, which is important for understanding the lignin polymerization and may shed some light on the development of efficient laccase-mediator systems.

Introduction

Laccases (EC 1.10.3.2, benzenediol: dioxygen oxidoreductases), ubiquitous multi-copper oxidases in fungi, plants and insects,[1] can use dioxygen in air as electron acceptor to oxidize a wide variety of substrates. A large number of biological roles of laccases have been identified including lignification,[2-4] delignification,[5] and cuticle sclerotization.[6] Also the application in environment science is appealing, especially for the bioremediation of phenolic-rich wastewater and polluted soils.[7] Furthermore, laccase can use small molecules (so called mediators) to facilitate the oxidation of species that would not normally be a substrate for the enzyme. Owing to its broad biotechnological issues and potential applications,[8] laccase-mediator systems (LMSs) have recently been extensively studied,[9-11] particularly since the seminal introduction of ABTS, 2,2'-azino-bis(3-ethylbenzothiazoline-6-sulphonic acid), which was discovered to be able to speed up the oxidation of non-phenolic substrates.[12] Meanwhile, plant metabolites[9,13,14] such as natural phenols have aroused scientists' enthusiasm as eco-friendly mediators, because of their low cost and toxicity compared to synthetic mediator compounds.[9] In general, LMSs are subject to a class of laccase-catalyzed oxidation on multiple substrates, in which numerous secondary reactions occur among reactive species generated by laccases and substrates.[11] However, compared to the electron transfer process in the multiple-copper center of laccases,[15,16] which has been investigated thoroughly for more than half of a century by both experiments and computations, the forming and evolving mechanisms of the natural phenol related reactive species, such as phenoxyl radical, remain unknown.

[a] State Key Laboratory of Microbial Metabolism, School of Life Sciences and Biotechnology, Shanghai Jiao Tong University, Shanghai, 200240.
[b] College of Urban and Environmental Sciences, Peking University, Beijing, 100871.
[c] Technical Center, Huabao Intl. Holdings, Shanghai, 201821.

† Electronic Supplementary Information (ESI) available: The EFA analysis results, plots of the EUG and ISO consuming rate verse concentration, the mass spectra of the intermediates and products, the transition states of HAT and RC reactions, the substrates, radical structures and detailed coordination, energy, frequency and spin density. See DOI: 10.1039/x0xx00000x

‡ These authors contribute equally to this work.

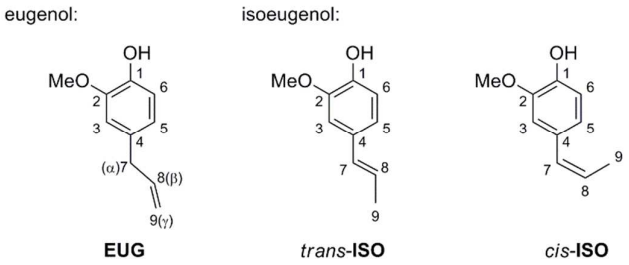

Scheme 1. Chemical structures of the two types of isomeric natural phenols, **EUG** and **ISO**.

Eugenol (**EUG**) and *trans-/cis*-isoeugenol (**ISO**), are two types of propenyl methoxyphenol metabolites in botanic lignin and lignan biosynthesis[17,18] (Scheme 1). **EUG** and **ISO** have highly analogous core structural characteristics with the elementary units of lignin, including an *o*-methoxy group adjacent to the phenolic hydroxyl group and a *para*-unsaturated group conjugating (or not) with the aromatic ring, which are also possessed by a significant number of recently discovered phenolic mediators.[19,20] *In vitro* experiments have shown that oxidation of **EUG** and **ISO** also leads to lignin-like polymers, implying similar reaction pathways.[21,22] Horseradish peroxidase (HRP) and 2,2-diphenyl-1-picrylhydrazyl (DPPH) radical catalyzed oxidation of **EUG** have been demonstrated to form a yellow-colored quinone methide intermediate and a dehydrodieugenol product,[23-25] while in the DPPH-catalyzed oxidation of **ISO**, dehydrodiisoeugenol and its nucleophilic adducts have been identified to be the main products,[23,26] suggesting that **EUG** and **ISO** could be used as excellent chemical probes to investigate the active intermediates and secondary reactions occurring in the enzymatic oxidation catalyzed by laccase.

In this work, the chemical kinetics and reaction mechanisms were firstly combined to uncover the diversity of laccase-catalyzed oxidation using **EUG** and **ISO** as chemical probes. Laccase from white rot fungus *Trametes Versicolor* was used to catalyze the oxidative processes of the two isomeric natural phenols, and particularly the derivative reactions beyond the *O*-centered phenol radicals were extensively investigated. Time-resolved UV-Vis absorbance spectra recorded the reaction kinetics, rapid HPLC-MS technique captured the relative stable reaction intermediates and products, and state-of-the-art quantum calculation rationalized the formation and evolution of these transient species suggested by auxiliary multicomponent analysis.

Experimental

Trametes Versicolor laccase (10 U/mg), ABTS (98%), **EUG** (99%), and **ISO** (98%, mixture of *cis*- and *trans*-forms) were purchased from Sigma-Aldrich Company. Stock solutions of **EUG** and **ISO** (0.99 mM) were prepared by dissolving the corresponding chemical in sodium citrate buffer (0.1 M, pH 5.0, acetonitrile : water = 1 : 4 in volume, for increasing solubility) and stored at 4 ºC. Typically, the reaction mixture contained 0.089 mM phenol substrates and 0.065 mg/ml laccase in the above buffer solution. The time-resolved UV-Vis absorbance spectra were immediately recorded in a range of 190-1100 nm with a 0.5 s interval by Agilent 8453 UV-Visible spectrophotometer, after rapidly blending the substrates and laccase, at ambient atmosphere and room temperature.

The Multivariate Curve Resolution-Alternating Least Squares (MCR-ALS) method[27,28] was used to analyze the chemical kinetic data recorded by the UV-Vis spectrophotometer. Basically, the raw data matrix $D(t, \lambda)$ was decomposed into time-dependent concentration matrix $C(t, n)$ and component-dependent absorbance coefficient matrix $S^T(n, \lambda)$,

$$D(t, \lambda) = C(t, n) \bullet S^T(n, \lambda) + E(t, \lambda) \quad (1)$$

where D, C, S^T, and E represent matrixes of the time-resolved raw data, resulting concentration, absorbance coefficients profiles, and residue not explained by the decomposition model, in terms of reaction time (t), wavelength (λ) and the number of components (n), respectively. The initial components concentration profile were estimated with Evolving Factor Analysis (EFA) algorithm,[28,29] which assumes that the measured signal is a linear combination of unresolved individual signals and performs principal components analysis on the data matrix along the time. To minimize ambiguity in mathematical resolution, we used Fast Fourier Transform algorithm (FFT) to truncate low signal-noise area in the raw data.[30] Then the time-resolved concentration profiles were used as constraint to develop the absorbance spectra. Finally, the time-resolved concentration data were fitted to the chemical dynamic profiles with DYNAFIT program,[31] and the MCR-ALS and DYNAFIT calculations were conducted back and forth to promote the analytic accuracy in the above mathematic treatment.

To characterize the intermediates and products, we guided 10 μL (injection volume) reaction solution to the rapid HPLC/UV-Vis-MS measurement at a certain time point. Retention time, UV-Vis absorbance of the mobile phase, and m/z signal for each component in the reaction mixture were monitored by Agilent 1290 High Performance Liquid Chromatograph (HPLC) with a diode array detector and coupled with Agilent 6230 Time-of-Flight (TOF) mass spectrometry. Agilent C18 reverse phase column (4.6 × 150 mm, 5 μm, Eclipse XDB-C18, Agilent, USA) was used in the HPLC instrument, and the mobile phase of acetonitrile and water (65% : 35% in volume) was eluted at 0.3 ml/min.

QM calculations were performed with Gaussian 09 program.[32] Bond dissociation energy of the phenolic hydroxyl groups in all possible monomeric reactants and intermediates and their relative energy differences were evaluated with the precise method of CBS-QB3. With an in-house developed "QM-based conformational search pipeline",[33,34] the branched reaction pathways after the primary O-H rupture were carefully constructed, and all of the involved stationary points were calculated at the M06/6-31++G** level and verified by frequency calculations. Solvent effects in water were then evaluated based on the PCM[35] and SMD[36] model. Molecular

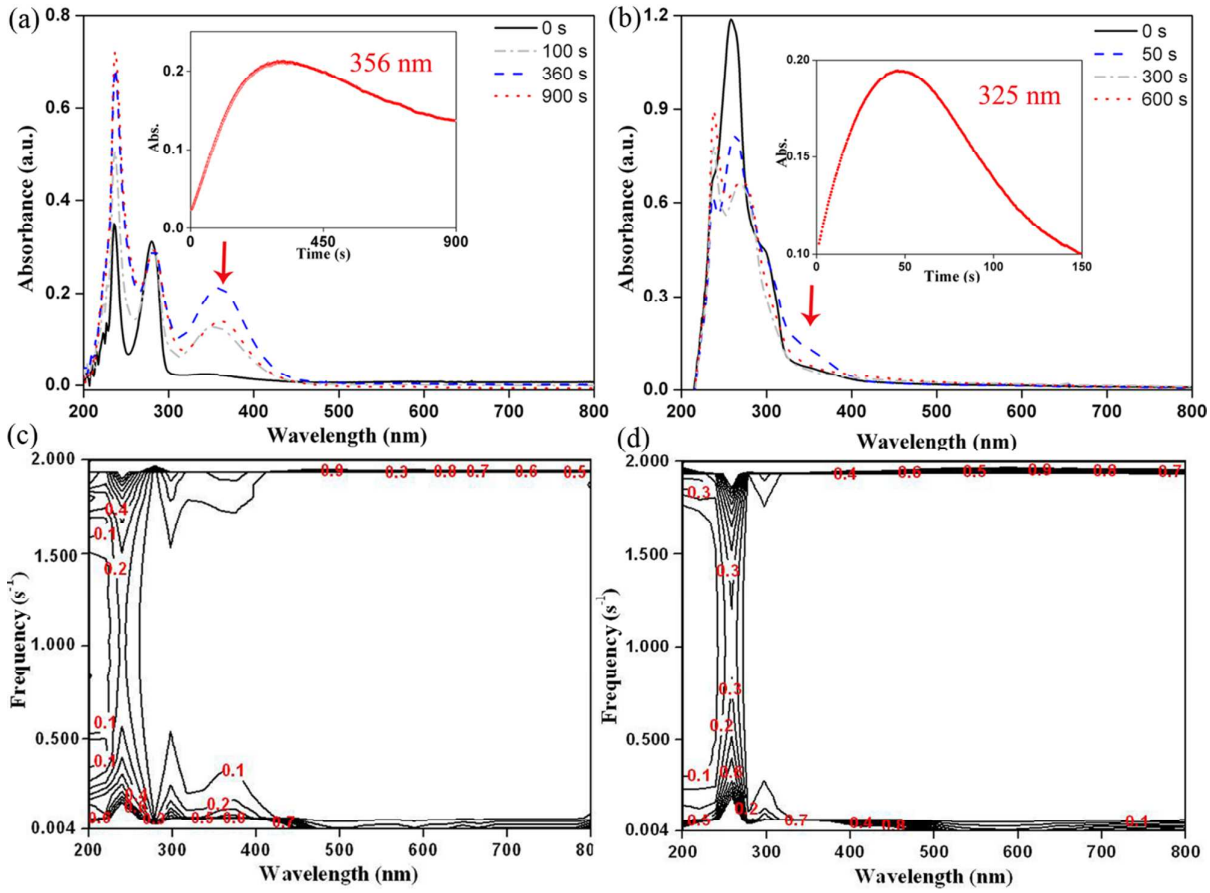

Figure 1. The time-resolved UV-Vis spectra of kinetic experiments and the corresponding FFT conversions in the cases of **EUG** (a and c) and **ISO** (b and d). The contour lines in (b) and (d) represent the amplitude after FFT conversions. Wavelength bands that have signals in the range of non-noisy frequencies are chosen for further MCR-ALS analysis.

spectra were also computed at the M06/6-31++G** level with the time-dependent DFT (TD-DFT) method.

Results and discussion

Kinetic Measurement

To explore the kinetic process of laccase-catalyzed oxidation of **EUG** and **ISO**, the absorbance changes were recorded at 0.5 s interval following the mixing of laccase and substrates. Figures 1a and 1b show the time-resolved UV-Vis spectra of **EUG** and **ISO** kinetic experiments. In the case of **EUG** (Figure 1a), the absorbance band remarkably increases at 236 nm and while the absorbance at 280 nm remains stable. It should also be noted that a nascent band at 356 nm rises in the early reaction stage and then decays gradually. As demonstrated in the inset, the 356 nm band reaches its maximum absorbance in about 310 seconds, accompanied with slightly blue-shift during the decaying. In the case of **ISO** (Figure 1b), the 257 nm absorbance band decreases continuously and disappears eventually, coupled with appearance of a new absorbance band at 240 nm. Also, a decline after rapid increment is observed in a range of 320 to 340 nm and its maximum absorbance obtained in 46 seconds at 325 nm is presented in the inset of Figure 1b.

MCR-ALS Analysis

Due to the severe overlaps of UV-Vis absorbance for different components in the kinetic experiments, it is necessary to decompose the raw kinetic data into the time-dependent absorbance for each component during the reaction time. To minimize the ambiguity of MCR-ALS analysis, FFT algorithm was used to abstract high-quality signal from the time-resolved UV-Vis spectra. The results obtained by FFT (Figure 1c and 1d) indicate that the applicable UV-Vis data lies in ranges of 230-270 nm and 290-400 nm in the case of **EUG**, and 230-340 nm in the case of **ISO**. Then the truncated kinetic data were resolved by model-independent MCR-ALS method. EFA suggests that the component numbers are three and four in the cases of **EUG** and **ISO** system, respectively, based on the principal components analysis of the data matrix along the time (Figure S1). However, the recommended component numbers might be smaller than the real ones, since some undistinguishable compounds, such as isomeric compounds probably possess similar UV-Vis absorbance and might be classified into one component.

The time-resolved normalized concentration profiles and corresponding absorbance coefficient profiles obtained by MCR-ALS analysis were plotted in Figure 2. The variance

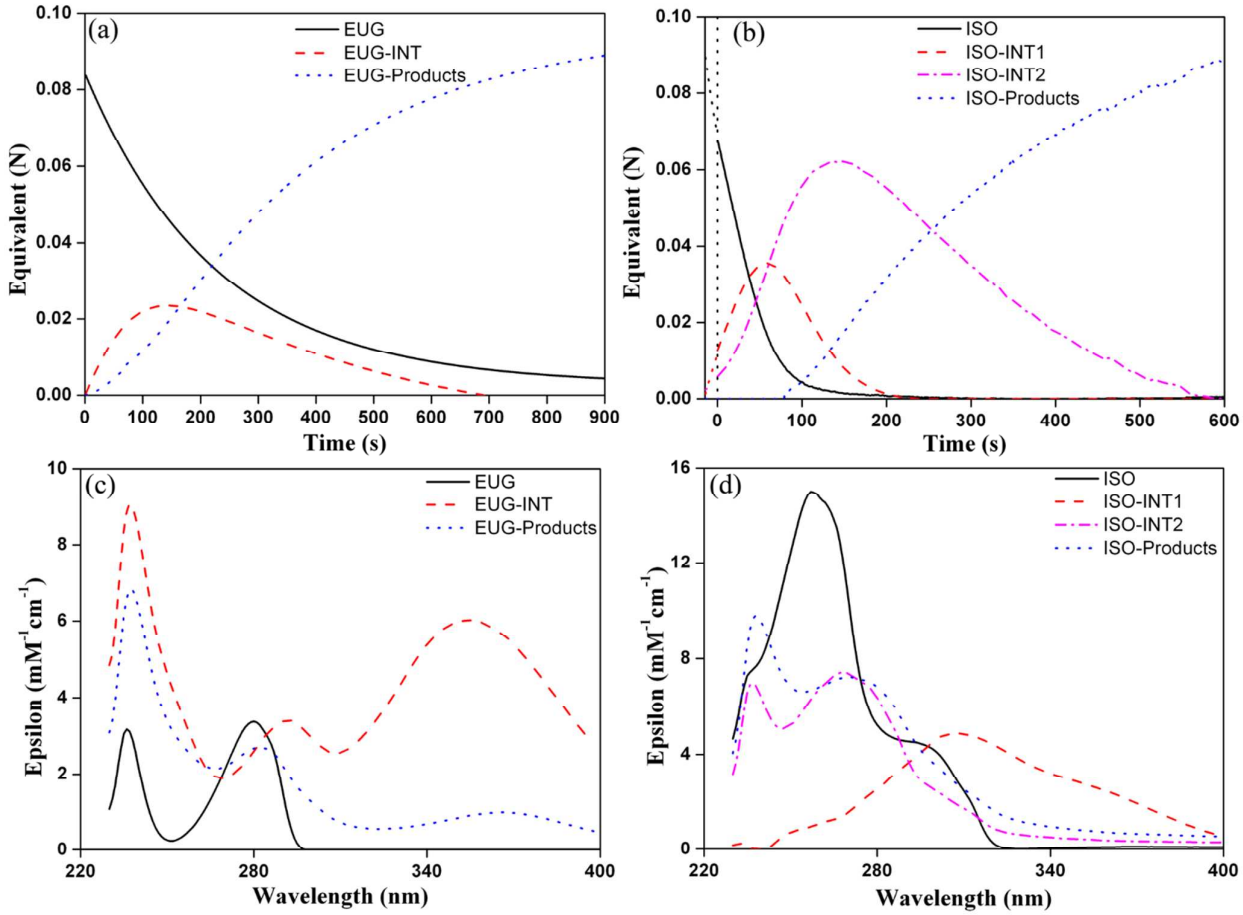

Figure 2. The MCR results of concentration and corresponding absorbance coefficient profiles, in the cases of **EUG** (a and c) and **ISO** (b and d).

explanations were 94.4% in **EUG** and 98.6% in **ISO**. It should be pointed out that in the case of **EUG** the time-dependent absorbance in the range of 271-289 nm was calculated with two constraints. One is the concentration profile obtained from the truncated kinetic data and the other is the common non-negativity and closure constraints. The validity and efficiency of the MCR-ALS analysis were assured by the consistency of the UV-Vis absorbance spectra of independent reactants and the component decomposed from the mixed UV-Vis spectra. In the case of **EUG**, the former consists of two peaks (236 and 280 nm) according with the latter (236 and 280 nm) very well; while in the case of **ISO**, the former includes one peak at 257 nm and a shoulder peak at 295 nm, agreeing with that at 257 and 295 nm (Figure 2c and 2d).

Hence, the MCR-ALS decomposition on the kinetic data and the time-resolved profiles were further used to analyze intermediates and products. According to the concentration profiles (Figure 2a and 2b), **EUG** is consumed in a time longer than 900 s and **ISO** is almost finished in just 200 s, which indicates that the catalytic degradation of **EUG** is much more slower than **ISO** in the reaction (consistent with the calculated BDEs in QM calculations section). Further, the consuming rate versus the substrates concentration was analyzed (Figure S2). The results show that the **EUG** consuming rate is linear with the concentration (Figure S2a), which indicates that a probably pseudo-first-order reaction dominates the reaction in the whole process. Interestingly, a nonlinear relationship between the consuming rate and the concentration was observed in the case of **ISO** (Figure S2b).

In the case of **EUG**, the emerging and decaying intermediate was resolved and resulted in absorption bands at 236, 291 and 355 nm, partially overlapped with the reactant (**EUG**) and possible products (the third component in the MCR-ALS decomposition). The intermediate reaches its maximum concentration at 144 s. In the case of **ISO**, two types of intermediates **ISO-INT1** and **ISO-INT2** were proposed. **ISO-INT1** with an absorption band at 310 nm has quite broad absorption in the range of 240-400 nm, and the absorption of **ISO-INT2** is similar to **ISO-Products** with absorbance bands at 236 and 268 nm, but with different intensities. **ISO-INT1** reaches its maximum concentrations at 57 s and **ISO-INT2** at 142 s. Especially, the **ISO-INT1** is likely to be the phenoxyl radical: since a rapid increase of absorption in the range of 300 to 400 nm was detected by the UV-Vis measurement and the TD-DFT (at M06/6-31++G** level) calculations presented two bands at 323 and 334 nm for the *cis*-**ISO**-generating and *trans*-**ISO**-generating phenoxyl radical (Figure 4b). The experimental observations are consistent with the theoretical calculations.

However, it is questionable whether **ISO-INT2** is one of the diverse products similar to **ISO-Products**.

Based on the MCR-ALS analysis, the possible intermediates and products are quite different in laccase-catalyzed oxidation of the two isomeric phenols, suggesting diverse pathways probably occurred during the oxidations.

HPLC-MS analysis

Considering the complexity of the oxidative processes and the limit of EFA analysis, the real number of species may be far from three and four in the laccase-catalyzed oxidation of **EUG** and **ISO**, respectively.[37] Thus, it is necessary to conduct the rapid HPLC-MS analysis and characterize the possible intermediates and products. The reaction mixtures were subjected to HPLC-MS analysis after certain reaction time: 300 s in the case of **EUG** and 180 s in the case of **ISO**. The resulting total ion chromatograms are shown in Figure 3, indicating at least 7 compounds (**A**-**G**) in the case of **EUG**, and 5 species (**A'**-**E'**) in the case of **ISO**. The possible chemical formula and relative abundance of each compound were listed in Table 1 and the mass spectra of the target peaks were shown in Figure S3-S4.

In the case of **EUG**, three groups of compounds with m/z = 163 $[M + H]^+$, 325 $[M + H]^+$, and 344 $[M + NH_4]^+$ were observed by the HPLC-MS analysis. The first group consists of compound **A** with m/z = 163 ($[C_{10}H_{10}O_2 + H]^+$) at retention time of 6.07 min (Figure 3a). Its fragmentation signals at m/z 131 and 103 are corresponding to de-methoxylation (32 u, CH_3OH) and de-ethylene (28 u, CH_2=CH_2) (Figure S3). The m/z and fragment signals indicate that compound **A** is likely to be a "eugenol quinone methide" species reported in previous literatures,[23,25,38,39] such as HRP and DPPH catalyzed oxidation of **EUG**. Moreover, theoretical analysis were used to evidence the identification of the eugenol quinone methide observed in this work. First, the TD-DFT calculations at the M06/6-31++G** level of theory demonstrate two bands of 220 and 360 nm for the eugenol quinone methide, which is consistent with the observed bands of 222 and 344 nm in HPLC/UV-Vis, as shown in Figure 4a. Second, not only MCR-ALS resolved **EUG-INT** spectra profile appears a strong absorbance at 355 nm in Figure 2c , but also an intermediate-like rapid increment and decay at 356 nm was detected (the inset of Figure 1a), in agreement with the UV-Vis spectra of compound **A** in Figure 4a. In conclusion, the critical intermediate of laccase-catalyzed oxidation of **EUG** was identified as the eugenol quinone methide by experimental and theoretical analysis.

Furthermore, a series of the dimeric isomers of eugenol quinone methide, composed of four compounds (**B**, **C**, **D** and **E**) with retention times of 7.44, 11.04, 11.34 and 14.58 min, were firstly characterized by mass spectra with m/z = 325 $[C_{20}H_{20}O_4 + H]^+$. Interestingly, the dimeric species ($C_{20}H_{20}O_4$, M_r = 324) are obviously beyond the previous range of products reported about the **EUG** oxidation, such as popular dehydrodieugenol ($C_{20}H_{22}O_4$, M_r = 326)[23,26] and self-nucleophilic adduct to eugenol quinone methide ($C_{20}H_{22}O_4$, M_r = 326).[40] The MS/MS analysis of m/z=325 showed a series of fragmentation signals

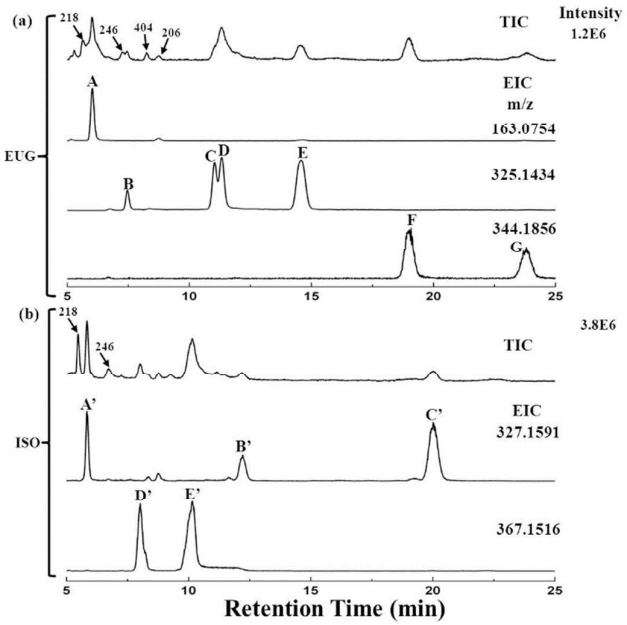

Figure 3. The total ion chromatogram and extracted ion chromatogram profiles in the cases of **EUG** (a) and **ISO** (b).

of 293, 261, 233, and 205, corresponding to the losses of 32 (CH3OH), 64 (2xCH3OH), 92 (2xCH3OH, C2H4), and 120 (2xCH3OH, 2xC2H4) of dimeric species. This indicated that the coupling might occur between two phenyl rings.

The third group includes compound **F** and **G** with retention time of 19.07 and 23.85 min and m/z = 344 characterized as $[C_{20}H_{22}O_4 + NH_4]^+$, probably corresponding to either dehydrodieugenol or self-nucleophilic adducts. The relative abundance was estimated to be 24: 2: 1: 32: 10: 17: 7 (**A**: **B**: **C**: **D**: **E**: **F**: **G**) based on the TIC peak areas in the HPLC trace.

In the case of **ISO**, the mixture of intermediates and products can briefly divide into two groups of compounds characterized by M_r = 326 and 344. The first group is composed of three compounds (**A'**, **B'** and **C'**, Figure 3b) with m/z =327 $[C_{20}H_{22}O_4 + H]^+$, and retention times of 5.83, 12.25 and 20.01 min, corresponding to either radical-radical coupling products (such as dehydrodiisoeugenol[23]) or radical-**ISO** coupling products, as shown in Scheme 3. The second group evidences two compounds (**D'** and **E'**, Figure 3b) with m/z = 367 $[C_{20}H_{24}O_5 + Na]^+$, and retention times of 8.02 and 10.20 min, probably corresponding to water adducts to the first group of compounds.[41] The relative abundance of those compounds was estimated to be 2: 1: 1: 1: 7 (**A'**: **B'**: **C'**: **D'**: **E'**). Unexpectedly, neither compound **A**-like eugenol quinone methide nor radical species was observed in the HPLC trace, even though the retention time of **A'** is very close to that of **A** in the HPLC trace. **A'**, **B'** and **C'** may be the products of *O*-centered phenoxyl radical coupling with another molecule of **ISO**, while **D'** and **E'** may be formed by nucleophilic addition of water to these dimeric species (**A'**-**C'**). The C8-O coupled quinone

methide, with the same chemical formula as dehydrodiisoeugenol, has been reported in the DPPH radical-mediated **ISO** oxidation,[23]

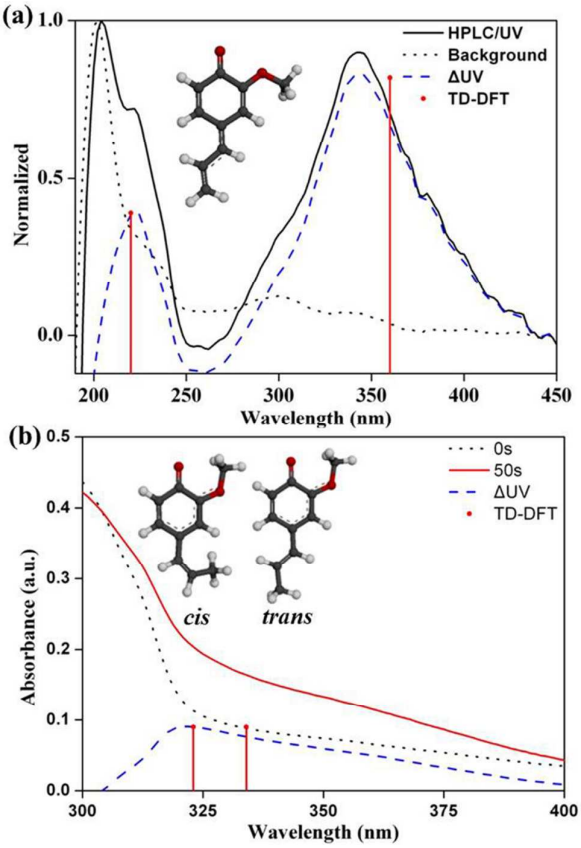

Figure 4. Comparison of the experimental and theoretical UV-Vis absorptions for the two intermediates: (a) The UV-Vis spectra of the HPLC mobile phase in the case of **EUG** at retention time = 6.07 min (solid line, corresponding to compound A), 6.4 min (dotted line, corresponding to the background absorption of the mobile phase) and the ΔUV (dashed line) obtained by subtracting background from the HPLC UV-Vis absorption and the TD-DFT calculated absorption bands (red bars) at the M06/6-31++G** level of theory. (b) The TD-DFT calculated absorption bands (red bars) for the cis- and trans-**ISO**-generating phenoxyl radicals and the detected absorption changes from 300 to 400 nm during 0~50 s (dashed line).

where the methanol adduct with M_r = 358 was detected in the GC-MS and HPLC-MS studies,[23] rather than the water adducts (**D'** and **E'**) observed in this work. Accordingly, in this work we suggested that in the kinetic analysis **ISO-INT2** might correspond to the group of dimeric species (**A'**, **B'**, and **C'**) and **ISO-Products** to the group of water adducts (**D'** and **E'**); unfortunately, the radical species (**ISO-INT1**) cannot be detected by the HPLC-MS method.

Therefore, quite a few intermediates and products were observed by the HPLC-MS analysis in the laccase-catalyzed oxidation of **EUG** and **ISO**. For **EUG**, a eugenol quinone methide intermediate with a typical absorption band at 356 nm was detected, and the dimeric isomers with M_r = 324 were firstly observed in this work. For **ISO**, however, only dimeric species and the water adducts were identified, in agreement with the literature.[23] All the experimental evidences

Table 1. The possible chemical formula and estimated abundance in the HPLC-MS analysis. (R.T./min, Peak Area/10^6 counts)

	Compound (R.T.)	m/z ESI(+)	Possible Formula	Calculated m/z	Peak Area
EUG	**A**(6.07)	163.0717	$C_{10}H_{10}O_2$+H^+	163.0754	9.4
	B(7.44)	325.1439	$C_{20}H_{20}O_4$+H^+	325.1434	0.8
	C(11.04)	325.1431	$C_{20}H_{20}O_4$+H^+	325.1434	0.4
	D(11.34)	325.1430	$C_{20}H_{20}O_4$+H^+	325.1434	13.0
	E(14.58)	325.1438	$C_{20}H_{20}O_4$+H^+	325.1434	4.3
	F(19.07)	344.1856	$C_{20}H_{22}O_4$+NH_4^+	344.1856	7.0
	G(23.85)	344.1853	$C_{20}H_{22}O_4$+NH_4^+	344.1856	2.9
ISO	**A'**(5.83)	327.1597	$C_{20}H_{22}O_4$+H^+	327.1591	8.8
	B'(12.25)	327.1598	$C_{20}H_{22}O_4$+H^+	327.1591	3.3
	C'(20.01)	327.1591	$C_{20}H_{22}O_4$+H^+	327.1591	4.5
	D'(8.02)	367.1511	$C_{20}H_{24}O_5$+Na^+	367.1516	4.6
	E'(10.20)	367.1510	$C_{20}H_{24}O_5$+Na^+	367.1516	26.0

demonstrated that oxidation of the two isomeric phenols experienced two diverse pathways and resulted in unlike intermediates and products.

Quantum Mechanical Calculations

To explore origin of the diversity of laccase-catalyzed oxidation, systematic quantum mechanical calculations were carried out for the two molecules of chemical probes. The first part of calculations was set out to determine the bond dissociation energies (BDEs)[42]. Although many factors influenced the oxidation rates of the isomeric phenols and corresponding radicals, the BDEs are related to the intrinsic reactivity of the oxidation.[43] The BDEs linked to *O*-centered phenoxyl radical (O-H bond) and *C*-centered allylic radical (Csp3-H) are calculated with CBS-QB3 method.

* calculated with the CBS-QB3 method

	BDEs (kcal/mol)*	
EUG		
	O-H	85.4
	propenyl C_{sp3}-H	77.8 (to *exo*- allylic)
		81.0 (to *endo*- allylic)
***cis*-ISO**		
	O-H	83.9
	propenyl C_{sp3}-H	84.2
***trans*-ISO**		
	O-H	82.9
	propenyl C_{sp3}-H	82.8
***endo*- Allylic**		
	O-H	62.2 (to *cis*-quinone methide)
	O-H	58.7 (to *trans*-quinone methide)
***exo*- Allylic**		
	O-H	62.0 (to *trans*-quinone methide)

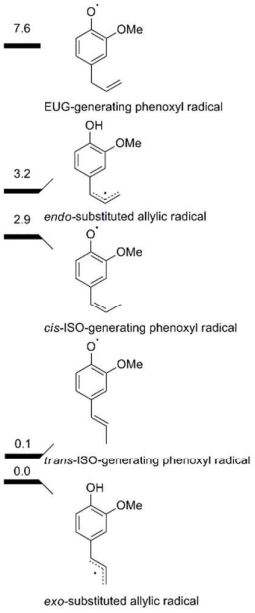

Scheme 2. The proposed diverse pathwasys for the laccase-catalyzed oxidation of EUG (a) and ISO(b).

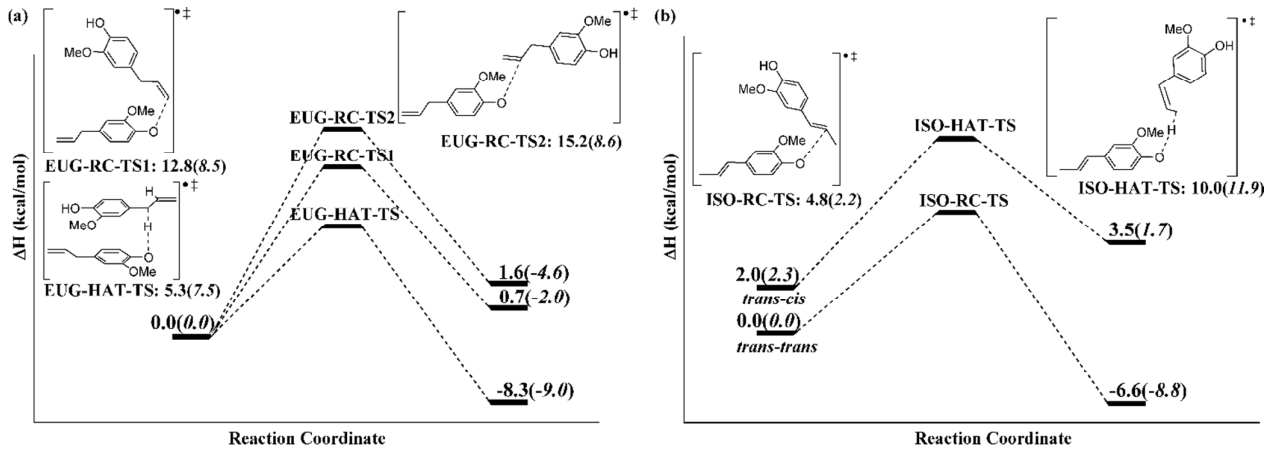

Figure 5. Comparison between the HAT and RC reactions of the laccase-generating phenoxyl radicals in the case of **EUG** (a) and **ISO** (b). The energy profiles were calculated at the M06/6-31++G** level of theory, and the solvent effect corrected energy were presented in parenthesis.

As shown in Scheme 2, the BDEs of O-H in **EUG**, *cis*-**ISO**, and *trans*-**ISO** are respectively calculated to be 85.4, 83.9, and 82.9 kcal/mol, in agreement with the experimental observation that **ISO** consumes faster than **EUG**. The BDEs of Csp3(α)-H bond in **EUG** to *exo*- and *endo*- allylic radicals are respectively 77.8 and 81.0 kcal/mol, indicating that the resulting phenoxyl radical is higher in energy than allylic radicals, by 4.4 – 7.6 kcal/mol. The BDE of the Csp3(γ)-H bond in *cis*-**ISO** is 84.2 kcal/mol, higher than the relative BDE of O-H bond by 0.3 kcal/mol, and the BDE of the Csp3(γ)-H bond in *trans*-**ISO** is 82.8 kcal/mol, 0.1 kcal/mol lower than the corresponding BDE of the O-H bond. It is nearly thermoneutral between the corresponding phenoxyl radicals and allylic radicals in the case of **ISO**. The significant energy gap indicates that **EUG**-generating *O*-centered phenoxyl radical could evolve to more stable *C*-centered allylic radical. Furthermore, the secondary oxidation from allylic radicals to quinone methide would be much easier for the lower BDEs of O-H bonds, in a range of 58.7 to 62.2 kcal/mol.

The second part of calculation was set out to unravel the fate of the nascent phenoxyl radicals. Here, we carefully calculated possible derivative reactions, including hydrogen atom transfer (HAT)[44] and radical coupling (RC) reactions among the available reactants and the nascent phenoxyl radicals. For HAT reactions, **EUG**- and **ISO**-generating phenoxyl radicals scramble the hydrogen atom of propenyl Csp3-H bond from **EUG** and **ISO**, converting into the *C*-centered allylic radicals. For RC reactions, **EUG**- and **ISO**-generating phenoxyl radicals couple with propenyl double bond and form oligomers.

In the case of **EUG** (Figure 5a), the lowest activation enthalpy of the HAT reaction is calculated to be 5.3 kcal/mol at the M06/6-31++G** level of theory, lower than the lowest activation enthalpy of the RC reaction by 7.5 kcal/mol, in which the phenoxyl radical attacks on the C(γ) position of the propenyl group and forms *C*-centered radical on the C(β) position; the activation energy increases when it couples the C(β) position, since the resulting *C*-centered radical is at the less-substituted C(γ) position. On the contrary, in the case of **ISO** (Figure 5b), the lowest activation enthalpy of the RC reactions is found to be 4.8 kcal/mol in *trans*-**ISO**, and the lowest activation enthalpy of the HAT reaction is 8.0 kcal/mol in *cis*-**ISO** (Figure S5). It is obvious that the RC reaction is easier than that of HAT by at least 3.2 kcal/mol. The computational results indicated that the two phenoxyl radicals undergo different pathways: the unstable **EUG**-generating *O*-centered phenoxyl radical evolves to stable *C*-centered allylic radical while the relatively stable **ISO**-generating *O*-centered radical couples with unsaturated double bond in the reactants to generate the dimeric species.

Figure 6a collected six low-energy transition states for the HAT reaction in the case of **EUG**, **EUG-HAT-TS1~6**, with activation enthalpies in a range of 5.3 to 9.1 kcal/mol. By comparing **EUG-HAT-TS1~3** with **EUG-HAT-TS4~6**, we can conclude that the π-π stacking interaction plays an important role in stabilizing the compact transition states. Besides, the influence of the propenyl rotation is found to be smaller. The methyl group would close the phenoxyl oxygen to avoid electrostatic repulsion between the two oxygen atoms. These transition states indicate that the HAT reactions lead to the formation of relatively stable *C*-centered exo-allylic radicals.

Figure 6b shows six low-energy transition state structures for the RC reactions with relatively stable *trans*-**ISO** species, which might be abundant in the oxidation owing to the smaller O-H BDEs (82.9 kcal/mol) than that of *cis*-**ISO** (83.9 kcal/mol). Similarly, the π-π stacking interaction plays important roles in **ISO-RC-TS1~4**, decreasing the activation enthalpy significantly. Interestingly, the *O*-centered phenoxyl radicals prefer to attacks on the C(β) position, with the small barrier of 4.8 kcal/mol, leading to a benzyl-type radical species. Similarly, for the RC reaction in the case of **EUG** the calculated barrier of the phenoxyl radical attacking on the C(β) position (12.8 kcal/mol) is lower than that of attacking on the C(γ) position (15.2 kcal/mol). It may be due to the less-conjugation

for the C(γ)-type radical-alkene coupling reaction. The transition state structures for the **EUG**-RC and **ISO**-HAT reactions are collected in Table S2-4.

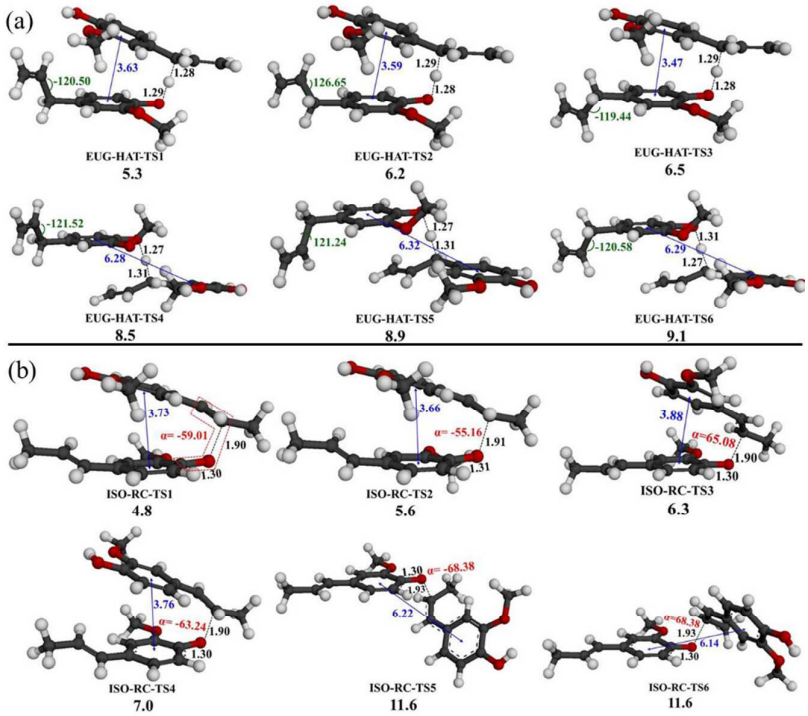

Figure 6. The low-energy transition structures of the **EUG-HAT** (a) and **ISO-RC** (b) reaction, optimized at the M06/6-31++G** level of theory. (activation enthalpies in kcal/mol and distances in Å).

Accordingly, the QM calculations indicate that two competitive pathways exist for the evolving of *O*-centered phenoxyl radicals and lead to diverse intermediates and products for **EUG** and **ISO**. In the case of **EUG**, the HAT reaction takes priority over the RC reaction, and on the contrary, the RC reaction probably dominated the secondary reactions in the case of **ISO**. The theoretical calculations explain why the quinone methides observed in HPLC-MS are in the monomeric form in the case of **EUG**, and the dimeric form in the case of **ISO**.

Mechanism Consideration

Based on the UV-Vis kinetic experiment, MCR-ALS mathematical analysis, rapid HPLC-MS measurement and QM calculations, the dominant pathways were constructed for the laccase-catalyzed oxidation of **EUG** and **ISO** (Scheme 3).

In the case of **EUG** (Scheme 3a), the nascent phenoxyl radical does mainly transform to the allylic radical via a HAT reaction. The conversion of *O*-centered phenoxyl radical to *C*-centered allylic radical seems to be opposite to our general concept;[45] however, the special stabilization of the allylic radical stems from the delocalization of unpaired electron among aromatic ring and double bond. Due to the lower BDEs of the O-H bond (Scheme 2), the resulting allylic radical further experiences the second oxidation and transform to eugenol quinone methide (i.e. **EUG-INT**, putatively compound **A**). The eugenol quinone methide is highly reactive and likely to dimerize through Diels-Alder reaction[46,47] or Domino reactions[48,49], leading to the formation of the dimeric species with molecular weight 324 (i.e. putatively compound **B**, **C**, **D**, **E**). What's more, dehydrodieugenol or eugenol adducts, with molecular weight of 326 (i.e. putatively compound **F**, **G**), may be generated by the directly coupling reaction of phenoxyl radicals and nucleophilic addition of eugenol quinone methide and **EUG**, respectively.

In the case of **ISO** (Scheme 3b), the nascent phenoxyl radical is captured by another molecule of **ISO** via the RC reaction at the C(β) position and leads to the formation of the benzyl radical, and thereafter the O-H bond from the adding **ISO** in the resulting benzyl radical also expected with a lower BDE. Considering the structure similarity of **ISO** with monolignols, it is more likely to couple via those kind of linkages such as Cβ-O and Cβ-Cβ (namely C8-O and C8-C8).[43] Similarly, the preference of forming the benzyl radical also stems from the delocalization of unpaired electron with the neighbouring aromatic ring. Then the benzyl radicals can be further oxidized into the dimeric form of quinone methides (i.e. **ISO-INT2**, putatively compound **A'**, **B'** and **C'**) with double molecular weight (M_r = 326). It is also interesting to observe the hydration for the quinone methides, with molecular weight of 344, in the case of **ISO**. Instead of the dimerization, the nucleophilic addition occurs dominantly, leading to the formation of water adducts such as **D'** and **E'**. The driving force for the water addition may attribute to the re-aromatization of

the dimeric form of quinone methides. Overall, this process regenerates phenol group and adds a hydroxyl group on the alkyl chain in the oligomeric species, probably responsible for

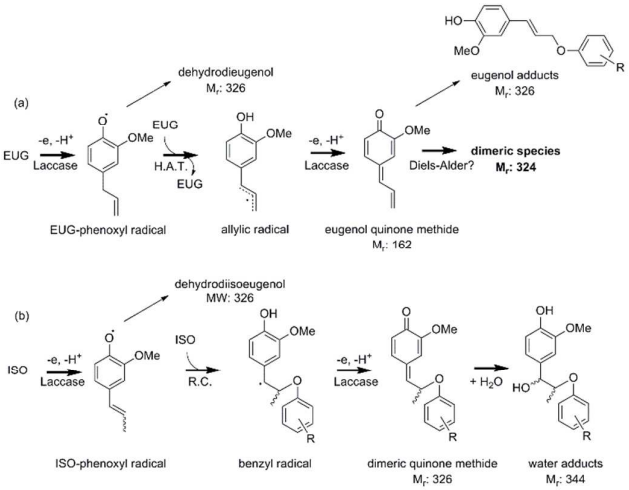

Scheme 3. The proposed diverse pathwasys for the laccase-catalyzed oxidation of EUG (a) and ISO(b).

molecular elongation in lignification. Furthermore, dehydrodiisoeugenol with molecular weight of 326 might present due to a radical coupling reaction between two phenoxyl radicals; however, this species is unlikely to react with water.

Notably, in the previous literatures, the observed quinone methide was attributed to the self-exchange disproportionation, a type of HAT between two phenoxyl radicals generated by laccase oxidation.[1,5,6] For example, Sugumaran *et al.* proposed a dismutation mechanism for the quinone methide formation from 2,6-dimethoxy-4-allyl phenol.[50] However, no radical species was observed in the **EUG** oxidation, indicating that **EUG** phenoxyl radical is in very low concentration. Even though it is undistinguishing in experiment whether it is the reaction between two phenoxyl radicals or phenoxyl radical and **EUG** in the formation of eugenol quinone methide, it is likely that the HAT reaction would occur between the nascent phenoxyl radical and another molecule of **EUG**, at least at the beginning stage with the higher concentration of **EUG**. Different from the **EUG** system, the relative stable **ISO**-generating phenoxyl radical may accumulate during the primary oxidation based on the MCR-ALS analysis. It is also found that the **ISO** consuming rate is nonlinear to its concentration, in particular at the high concentration (> 0.03 mM, Figure S2), evidencing that multiple molecules of **ISO** involves in the reactions with the radical intermediate.

The experimental and theoretical results about HAT and RC reactions are in agreement with observations in the previous literatures. Firstly, the HAT reaction have been studied in the LMSs such as in the cases of HBT[51] or HPI.[52] HAT mechanism was also proposed for natural phenols and lignin-derived compounds mediated oxidation of lignin or recalcitrant compounds, by attacking the benzylic C(α)-H bond.[13,53] Moreover, a phenoxyl radical mediated α/β HAT reaction in the pyrolysis of phenethyl phenyl ether (PPE), the simplest model of lignin linkage unit, has also been systematically studied experimentally and computationally.[54-56] Secondly, the phenoxyl radical mediated RC mechanism has been proposed in the coupling of monolignols.[43] The monolignol radicals can attack on the C(α) or C(β) position of the unsaturated double bond[43] and promotes the formation of complex lignin structure by oxidative coupling.[57-59]

Conclusions

Natural phenols have been used as mediator molecules in the LMSs, though many detailed mechanisms are still unclear. Two types of isomeric natural phenols (**EUG** and **ISO**) were employed as chemical probes to explore the mechanisms in the laccase-catalyzed oxidation. First, the kinetic experiments and MCR-ALS analysis indicate that the consuming rate of **EUG** is almost linear with its concentration along the time but non-linear in the case of **ISO**, implying that the two chemical probes undergo different reaction pathways in the laccase-catalyzed oxidation. Second, diverse intermediates and products were identified with the UV-Vis experiment, HPLC-MS measurement and TD-DFT calculations. Among them, two transient intermediates, an **EUG**-generating o-methoxy quinone methide intermediate, ((E/Z)-4-allylidene-2-methoxycyclohexa-2,5-dienone), and a **ISO**-generating phenoxyl radical, ((E/Z)-2-methoxy-4-(prop-1-en-1-yl) phenoxyl radical), were detected spectroscopically and computationally. Besides, the eugenol quinone methide and the corresponding dimeric products, and the dimeric form of **ISO** quinone methide and the corresponding water adducts were all captured by mass spectra. Third, the derivative reactions for **EUG** and **ISO** can be rationalized from different destinies of *O*-centered phenoxyl radical based on the QM calculations. The BDE calculations indicate that **EUG**-generating *O*-centered radical (85.4 kcal/mol) might evolve to stable *C*-centered allylic radical (77.8 and 81.0 kcal/mol in *exo*- and *endo*-allylic radicals) and be followed by the second oxidation to eugenol quinone methides, while **ISO**-generating *O*-centered radical (83.9 amd 82.9 kcal/mol in *cis*- and *trans*-**ISO**) and *C*-centered allylic radical (84.2 amd 82.8 kcal/mol in *cis*- and *trans*-**ISO**) are thermoneutral and thereby the phenoxyl radical cumulates for the RC reaction. Furthermore, the QM calculations indicate that in the case of **EUG**, the HAT reaction with the lowest activation enthalpies of 5.3 kcal/mol takes priority over the RC reaction. In contrast, the RC reaction attacking the C(β) position resulted in the formation of *C*-centered benzyl radical with the barrier of 4.8 kcal/mol probably dominated in the case of **ISO**. The special stabilization of the allylic radical and benzyl radical can be stems from delocalization of unpaired electron among phenyl ring and double bond. This suggests that the reactive species can be generated by radical conversion. These studies of **EUG** and **ISO** provide insights into the chemical nature of phenolic radicals, which plays a critical role in the natural process of phenolic radical polymerization such as lignification[60], and serve as the basis for further research to

illustrate other important factors in lignification[59], e.g. the interactions between laccase and reactive intermediates. The present work can also be helpful in the discovery of high-efficiency natural mediators and promote the application of eco-friendly laccase in industry.

Acknowledgements

This work was supported by National High-Tech R&D Program of China "863" (No. 2012AA020403) and the National Basic Research Program of China "973" (Nos. 2012CB721005, 2013CB966802), National Science Foundation of China (Nos. 21377085, 21303101), MOE New Century Excellent Talents in University (No. NCET-12-0354), and the SJTU-HPC computing facility award.

Notes and references

Abbreviations:
ABTS, 2,2'-azino-bis(3-ethylbenzothiazoline-6-sulphonic acid); **BDE**, bond dissociation energy; **CBS**, complete basis set; **DFT**, density functional theory; **DPPH**, free radical 2,2-diphenyl-1-picrylhydrazyl; **EFA**, evolving factor analysis; **EIC**, extracted ion chromatogram; **EUG**, eugenol; **FFT**, Fast Fourier Transform; **GC**, gas chromatography; **HAT**, hydrogen atom transfer; **HBT**, 1-hydroxybenzotriazole; **HPI**, N-hydroxyphthalimide; **HPLC**, high performance liquid chromatograph; **HRP**, Horseradish peroxidase; **ISO**, isoeugenol; **LMS**, laccase-mediator system; **MCR-ALS**, Multivariate Curve Resolution-Alternating Least Squares; **MS**, mass spectrometry; **PPE**, phenethyl phenyl ether; **TD-DFT**, time-dependent DFT; **TOF**, Time-of-Flight; **QM**, quantum mechanistic; **RC**, radical coupling; **TIC**, total ion chromatogram; **UV-Vis**, ultra-violet-visible.

1 P. Strong and H. Claus, *Crit. Rev. Env. Sci. Technol.*, 2011, **41**, 373–434.
2 W. Bao, D. M. O'malley, R. Whetten, and R. R. Sederoff, *Science*, 1993, **260**, 672–674.
3 L. B. Davin, H. B. Wang, A. L. Crowell, D. L. Bedgar, D. M. Martin, S. Sarkanen, and N. G. Lewis, *Science*, 1997, **275**, 362–367.
4 Y. Y. Wan, T. Miyakoshi, Y. M. Du, L. J. Chen, J. M. Hao and J. F. Kennedy, *Int. J. Biol. Macromol.*, 2012, **50**, 530–533.
5 C. F. Thurston, *Microbiology*, 1994, **140**, 19–26.
6 P. Giardina, V. Faraco, C. Pezzella, A. Piscitelli, S. Vanhulle and G. Sannia, *Cell. Mol. Life Sci.*, 2010, **67**, 369–385.
7 Y. Dai, L. Yin and J. Niu, *Environ. Sci. Technol.*, 2011, **45**, 10611–10618.
8 S. Rodríguez Couto and J. L. Toca Herrera, *Biotechnol. Adv.*, 2006, **24**, 500–513.
9 C. Johannes and A. Majcherczyk, *Appl. Environ. Microbiol.*, 2000, **66**, 524–528.
10 H. Call and I. Mücke, *J. Biotechnol.*, 1997, **53**, 163–202.
11 M. Fabbrini, C. Galli and P. Gentili, *J. Mol. Catal. B: Enzym.*, 2002, **16**, 231–240.
12 R. Bourbonnais and M. G. Paice, *FEBS Lett.*, 1990, **267**, 99–102.
13 S. Camarero, D. Ibarra, M. J. Martínez and Á. T. Martínez, *Appl. Environ. Microbiol.*, 2005, **71**, 1775–1784.
14 G. Andreu and T. Vidal, *Bioresour. Technol.*, 2013, **131**, 536–540.
15 S. K. Lee, S. D. B. George, W. E. Antholine, B. Hedman, K. O. Hodgson and E. I. Solomon, *J. Am. Chem. Soc.*, 2002, **124**, 6180–6193.
16 E. I. Solomon, J. W. Ginsbach, D. E. Heppner, M. T. Kieber-Emmons, C. H. Kjaergaard, P. J. Smeets, L. Tian and J. S. Woertink, *Faraday Discuss.*, 2010, **148**, 11–39.
17 T. Koeduka, E. Fridman, D. R. Gang, D. G. Vassão, B. L. Jackson, C. M. Kish, I. Orlova, S. M. Spassova, N. G. Lewis and J. P. Noel, *Proc. Natl. Acad. Sci. U. S. A.*, 2006, **103**, 10128–10132.
18 D. R. Gang, J. Wang, N. Dudareva, K. H. Nam, J. E. Simon, E. Lewinsohn and E. Pichersky, *Plant Physiol.*, 2001, **125**, 539–555.
19 A. I. Cañas and S. Camarero, *Biotechnol. Adv.*, 2010, **28**, 694–705.
20 T. Rosado, P. Bernardo, K. Koci, A. V. Coelho, M. P. Robalo and L. O. Martins, *Bioresour. Technol.*, 2012, **124**, 371–378.
21 A. Salanti, M. Orlandi, E. L. Tolppa and L. Zoia, *Int. J. Mol. Sci.*, 2010, **11**, 912–926.
22 S. Siegei, P. Frost and F. Porto, *Plant Physiol.*, 1960, **35**, 163–167.
23 R. Bortolomeazzi, G. Verardo, A. Liessi and A. Callea, *Food Chem.*, 2010, **118**, 256–265.
24 C. Bouhlel, G. A. Dolhem, X. Fernandez and S. Antoniotti, *J. Agric. Food Chem.*, 2012, **60**, 1052–1058.
25 D. Thompson, K. Norbeck, L. Olsson, D. Constantin-Teodosiu, J. Van der Zee and P. Moldeus, *J. Biol. Chem.*, 1989, **264**, 1016–1021.
26 L. Hernandez-Vazquez, M. T. D. Olivera-Flores, F. Ruiz-Teran, I. Ayala and A. Navarro-Ocana, *J. Mol. Catal. B: Enzym.*, 2011, **72**, 102–106.
27 R. Tauler, *Chemom. Intell. Lab. Syst.*, 1995, **30**, 133–146.
28 J. Jaumot, R. Gargallo, A. de Juan and R. Tauler, *Chemom. Intell. Lab. Syst.*, 2005, **76**, 101–110.
29 M. Maeder, *Anal. Chem.*, 1987, **59**, 527–530.
30 L.-X. Liu and Y.-L. Zhao, *Chinese Software Registration*, 2013SR100504, 2013.
31 P. Kuzmic, *Methods Enzymol.*, 2009, **467**, 247–280.
32 M. J. Frisch, *et al.*, Gaussian 09 (Revision A.02), Gaussian, Inc., Wallingford, CT, 2009.
33 Y.-L. Zhao, J. Yan and Z. Xu, *Chinese Software Registration*, 2012SR110566, 2012.
34 Z. Xu and Y.-L. Zhao, *Chinese Software Registration*, 2011SR077761, 2011.
35 J. Tomasi, B. Mennucci and R. Cammi, *Chem. Rev.*, 2005, **105**, 2999–3093.
36 A. V. Marenich, C. J. Cramer and D. G. Truhlar, *J. Phys. Chem. B*, 2009, **113**, 6378–6396.
37 A. Jayaraman, R. Tauler and A. de Juan, *J. Chromatogr. B*, 2012, **910**, 138–148.
38 D. C. Thompson, J. A. Thompson, M. Sugumaran and P. Moldéus, *Chem.Biol. Interact.*, 1993, **86**, 129–162.
39 W. J. Bodell, Q. Ye, D. N. Pathak and K. Pongracz, *Carcinogenesis*, 1998, **19**, 437–443.
40 A. Turner, *Chem. Soc. Rev.*, 1964, **18**, 347–360.
41 J. Ralph, P. F. Schatz, F. Lu, H. Kim, T. Akiyama and S. F. Nelsen, in *Quinone methides*, ed. S. E. Rokita, Wiley-Interscience: Hoboken, 2009, vol. 1, ch. 12, pp. 385.
42 R. Parthasarathi, R. A. Romero, A. Redondo and S. Gnanakaran, *J. Phys. Chem. Lett.*, 2011, **2**, 2660–2666.
43 A. K. Sangha, J. M. Parks, R. F. Standaert, A. Ziebell, M. Davis and J. C. Smith, *J. Phys. Chem. B*, 2012, **116**, 4760–4768.
44 A. Sirjoosingh and S. Hammes-Schiffer, *J. Phys. Chem. A*, 2011, **115**, 2367–2377.
45 J. Bartalis, Y.-L. Zhao, J. W. Flora, J. B. Paine III and J. B. Wooten, *Anal. Chem.*, 2008, **81**, 631–641.

46 S. Witayakran, A. Zettili and A. Ragauskas, *Tetrahedron Lett.*, 2007, **48**, 2983–2987.
47 S. Witayakran and A. J. Ragauskas, *Adv. Synth. Catal.*, 2009, **351**, 1187–1209.
48 S. Hajdok, J. Conrad and U. Beifuss, *J. Org. Chem.*, 2011, **77**, 445–459.
49 S. Hajdok, J. Conrad, H. Leutbecher, S. Strobel, T. Schleid and U. Beifuss, *J. Org. Chem.*, 2009, **74**, 7230–7237.
50 M. Sugumaran and J. L. Bolton, *Arch. Biochem. Biophys.*, 1998, **353**, 207–212.
51 P. Brandi, C. Galli and P. Gentili, *J. Org. Chem.*, 2005, **70**, 9521–9528.
52 G. Cantarella, C. Galli and P. Gentili, *J. Mol. Catal. B: Enzym.*, 2003, **22**, 135–144.
53 F. d'Acunzo and C. Galli, *Eur. J. Biochem.*, 2003, **270**, 3634–3640.
54 A. Beste, A. Buchanan III, P. F. Britt, B. C. Hathorn and R. J. Harrison, *J. Phys. Chem. A*, 2007, **111**, 12118–12126.
55 A. Beste, A. Buchanan III and R. J. Harrison, *J. Phys. Chem. A*, 2008, **112**, 4982–4988.
56 A. Beste and A. Buchanan III, *Energy Fuels*, 2010, **24**, 2857–2867.
57 K. V. Sarkanen and C. H. Ludwig, in *Lignins: occurrence, formation, structure and reactions*, Wiley-Interscience: New York, 1971, 916.
58 K. Freudenberg, *Nature*, 1959, **183**, 1152–1155.
59 W. Boerjan, J. Ralph and M. Baucher, *Annu. Rev. Plant Biol.*, 2003, **54**, 519–546.
60 R. Vanholme, B. Demedts, K. Morreel, J. Ralph and W. Boerjan, *Plant Physiol.*, 2010, **153**, 895–905.